HHS Public Access

Author manuscript

Nature. Author manuscript; available in PMC 2014 December 26.

Published in final edited form as:

Nature. 2014 June 26; 510(7506): 560–564. doi:10.1038/nature13409.

Structural rearrangements of a polyketide synthase module during its catalytic cycle

Jonathan R. Whicher[1,2,*], **Somnath Dutta**[1,*], **Douglas A. Hansen**[1,3], **Wendi A. Hale**[4], **Joseph A. Chemler**[1], **Annie M. Dosey**[1], **Alison R. Narayan**[1], **Kristina Håkansson**[4], **David H. Sherman**[1,3,4,5], **Janet L. Smith**[1,6], and **Georgios Skiniotis**[6]

[1]Life Sciences Institute, University of Michigan, Ann Arbor, MI 48109, USA

[2]Chemical Biology Graduate Program, University of Michigan, Ann Arbor, MI 48109, USA

[3]Department of Medicinal Chemistry, University of Michigan, Ann Arbor, MI 48109, USA

[4]Department of Chemistry, University of Michigan, Ann Arbor, MI 48109, USA

[5]Department of Microbiology & Immunology, University of Michigan, Ann Arbor, MI 48109, USA

[6]Department of Biological Chemistry, University of Michigan, Ann Arbor, MI 48109, USA

Abstract

The polyketide synthase (PKS) mega-enzyme assembly line uses a modular architecture to synthesize diverse and bioactive natural products that often constitute the core structures or complete chemical entities for many clinically approved therapeutic agents[1]. The architecture of a full-length PKS module from the pikromycin pathway creates a reaction chamber for the intra-module acyl carrier protein (ACP) domain that carries building blocks and intermediates between acyltransferase (AT), ketosynthase (KS), and ketoreductase (KR) active sites (see accompanying paper by Dutta *et al.*). Here we determined electron cryo-microscopy (cryo-EM) structures of a full-length PKS module in three key biochemical states of its catalytic cycle. Each biochemical state was confirmed by bottom-up liquid chromatography Fourier transform ion cyclotron resonance mass spectrometry (LC/FT-ICR MS). The ACP domain is differentially and precisely positioned after polyketide chain substrate loading on the active site of KS, after extension to the β-keto-intermediate, and after β-hydroxy product generation. The structures reveal the ACP dynamics for sequential binding to catalytic domains within the reaction chamber, and for transferring the elongated and processed polyketide substrate to the next module in the PKS

Correspondence to: Janet L. Smith; Georgios Skiniotis.

*These authors have contributed equally

Author contributions:

J.R.W. produced PikAIII variants and conducted enzyme assays. S.D. carried out cryo-EM data collection and processing. A.M.D. assisted with cryo-EM image processing. W.A.H, A.R.N. and K.H. carried out mass-spectrometry analysis. D.A.H. synthesized the thiophenol-pentaketide substrate. J.A.C. produced initial PikAIII samples. S.D., J.R.W., J.L.S. and G.S. analyzed the data and interpreted results. D.H.S., J.L.S. and G.S. designed research. J.R.W., S.D., D.H.S., J.L.S. and G.S. wrote the manuscript.

Supporting information

The cryo-EM maps have been deposited in the Electron Microscopy Data Bank (EMDB) with accession codes EMD-5663 (pentaketide-KS5-PikAIII), -5664 (β-ketohexaketide-PikAIII), -5665 (β-hydroxyhexaketide-PikAIII conformation i), -5666 (β-hydroxyhexaketide-PikAIII conformation ii), and-5667 (β-hydroxyhexaketide-PikAIII conformation iii).

pathway. During the enzymatic cycle the KR domain undergoes dramatic conformational rearrangements that enable optimal positioning for reductive processing of the ACP-bound polyketide chain elongation intermediate. These findings have crucial implications for the design of functional PKS modules, and for the engineering of pathways to generate pharmacologically relevant molecules.

Modular PKSs produce chemically diverse polyketide natural products that account for a large number of pharmaceutical compounds[1]. The modular organization of these enzyme assembly lines provides significant opportunities for synthetic biology applications and bioengineering[2–4]. However, many combinatorial biosynthesis efforts have been beset by problems of inefficiency and a limited ability to display "plug and play" behavior[5–7]. Thus, there is a critical need to dissect and understand the bacterial type I PKS module architecture and its conformational dynamics during polyketide chain elongation and processing.

Each module in the bacterial type I PKS catalyzes the elongation of an intermediate by two carbon atoms in a linear sequence, and may also modify the intermediate by reductive processing or β-branching[8]. An ACP domain within each module shuttles extender units and polyketide chain elongation intermediates between the catalytic domains. In an accompanying paper (Dutta *et al.*), we described the overall architecture of PKS module 5 (PikAIII) from the pikromycin pathway (Pik)[9]. This PKS module is organized around a dimeric KS domain and a central chamber for the ACP, with the active sites of catalytic domains facing the chamber. Here we examined the dynamics of ACP_5 within the reaction chamber of PikAIII in order to probe its localization and underlying protein-protein interactions during the catalytic cycle. Within PikAIII, AT_5 loads ACP_5 with a methylmalonyl (MM) extender unit, and KS_5 catalyzes a decarboxylative condensation reaction between the MM group and the pentaketide delivered by the module 4 ACP to produce a β-ketohexaketide intermediate. The β-hydroxyhexaketide product is subsequently generated through NADPH-dependent reduction by the KR_5 domain of PikAIII.

Incubation of full-length holo-PikAIII with thiophenol-pentaketide[10] generated pentaketide-PikAIII, in which this natural substrate was bound to the catalytic Cys209 of KS_5 (Extended Data Fig. 1a–c). The 3D cryo-EM map of pentaketide-KS_5-PikAIII was calculated at a resolution of 7.9 Å (Extended Data Fig. 2a,d), enabling precise docking of the structures of 6-deoxyerythronolide B (DEBS) module 5 KS and AT[11], DEBS module 1 KR[12], and DEBS module 2 ACP[13]. This EM reconstruction revealed several striking conformational changes compared to the structure of holo-PikAIII (Fig. 1a) (Dutta *et al.*). The AT_5 moves towards KS_5 by ~2 Å and partially occludes the side entrance to the KS_5 active site (Extended Data Fig. 3a), which may sequester the labile polyketide intermediateuntil the extension reaction occurs. In addition, several loops on the KS surface appear to have changed position and additional densities appear at the bottom of the KS, below the catalytic Cys209 (Extended Data Fig. 3a,b). These KS conformational changes upon pentaketide loading on Cys209 may be allosterically sensed by the AT domains, leading to the AT_5 shift. Pentaketide-induced conformational changes are also evident in the position of ACP_5, which shifts 10 Å and 30 Å towards AT_5 from its positions in the two holo-PikAIII conformers (Dutta *et al.*). In this position ACP_5 appears to insert helix 2 between two helices of the AT_5 lid subdomain (Fig.

1b). The interaction requires small conformational changes to one or both domains, although the details are not discernable in the EM maps. The reactive Ser1438 of ACP_5 is directed towards the AT_5 active site, presumably poising the ACP for loading with the MM extender unit by the AT domain. We probed the ACP-AT interface with single alanine substitutions in the AT_5 of the PikAIII-TE protein used for functional assays[14, 15] (PikAIII fused to PikAIV TE, the module 6 thioesterase domain). AT_5 Glu735 is in the ACP_5 contact zone, while Arg747, approximately 20 Å from the AT_5 active site, was predicted to reside in the ACP docking site of a DEBS AT[16]. Consistent with the cryo-EM results, the E735A or the R747A PikAIII-TE mutants exhibited ten-fold and five-fold reduced formation of the 10-dml macrolactone product, respectively (Extended Data Fig. 4).

The most surprising feature of the pentaketide-KS_5-PikAIII structure is that KR_5 has undergone an end-to-end flip compared to the holo-PikAIII reconstruction (Fig. 1c). This finding suggests that the pentaketide-induced repositioning of AT_5 and ACP_5 also affects the AT_5-KR_5 linker, causing the large rotation of KR_5. The end-to-end flip does not tangle the PikAIII topology, as the linker connections (residues 916 and 1360) are adjacent in KR_5 and reside at the junction of the structural (KR_{5struc}) and catalytic (KR_{5cat}) sub-domains. The ~180° KR_5 rotation positions the catalytic domain proximal to AT_5, with the AT_5-KR_5 interface formed by an AT_5 helix and two KR_{5cat} helices. Specifically, KR_5 Arg1133 and His1137 are positioned to interact with AT_5 Glu766 or Glu768. We confirmed the importance of the KR_{5cat}/AT_5 interface to catalytic function with R1133E, H1137E, E766R, and E768R substitutions, which had two- to fifteen-fold reduced activity relative to the wild-type PikAIII-TE (Extended Data Fig. 4). By contrast, substitution of a KR_{5struc} residue at the KR_{5struc}/AT_5 interface of holo-PikAIII had no impact on production of 10-dml (Dutta *et al.*). The end-to-end KR_5 flip, together with the unrelated repositioning of KR_5 observed upon ACP_5 deletion (Dutta *et al.*), indicates that its orientation depends on the state of other PikAIII domains.

To characterize the architecture of PikAIII in which the β-ketohexaketide chain elongation intermediate is tethered to ACP_5 we incubated holo-PikAIII with both MM-CoA and thiophenol-activated pentaketide (Extended Data Fig. 1d–i). The 3D cryo-EM structure of β-ketohexaketide-PikAIII at 7.8-Å resolution (Extended Data Fig. 2b,d) reveals the same overall PikAIII conformation of the catalytic domains as observed for pentaketide-KS-PikAIII, with the KR_5 catalytic domain proximal to AT_5 (Fig. 2a). Furthermore, in the β-ketohexaketide-PikAIII structure, AT_5 is significantly shifted towards KS_5 by 8 Å compared to the holo state and occludes the KS_5 side entrance (Fig. 2b), likely preventing intermediate transfer from the upstream PikAII ACP_4 to the KS_5 active site.

KR domains catalyze the NADPH-dependent reduction of the β-keto group to form either a D-(B-type KR) or L- (A-type KR) hydroxyl group. To form the two hydroxyl group stereochemistries, A- and B-type KRs are proposed to guide substrates into their active sites from opposite directions[17, 18] through the differential ordering of the KR “lid loop” and “lid helix” upon cofactor and substrate binding.[19] The β-ketohexaketide ACP_5 docks with the “lid helix” and “lid loop” of the A-type KR_5 with ACP_5 Ser1438 pointing towards the KR_5 active site at a distance of 19 Å (Fig. 2c). Given the long linker between KR and ACP (43 amino acids), it is unclear whether ACP_5 interacts with the KR_5 of the same or the opposite

monomer. An R1308E substitution in the KR_5 lid helix reduced activity 10-fold compared to wild type, validating the observed docking site (Extended Data Fig. 4a,b). From this position, a β-keto ACP substrate can enter the KR active site from either direction, facilitating formation of β-hydroxy products of KR-specified chirality[18]. Thus, the observed ACP-KR docking site is a general solution for PKS modules with either A- or B-type KRs.

To form β-hydroxyhexaketide-PikAIII, we incubated holo-PikAIII with MM-CoA, thiophenol-activated pentaketide, and NADPH (Extended Data Fig. 1j) and applied cryo-EM to obtain its structure. During initial 3D reconstructions we observed three different positions for ACP_5 and applied multiple-reference-supervised classification to calculate three independent 3D reconstructions at resolutions of ~11 Å (Fig. 3a and Extended Data Fig. 2c,d)[20, 21]. In all three conformers the catalytic domains are identically positioned, with the KS_5 side entrance occluded and the KR_5 domain oriented with its active site proximal to AT_5, as is the case with the pentaketide-PikAIII and β-ketohexaketide-PikAIII structures. In each conformer the ACP_5 domains are below the KR_{5struc} and completely outside the catalytic chamber (Fig. 3b). The ACP structure can be precisely docked within each corresponding density in all three states, indicating that the three positions are highly populated and that there is not significant ACP_5 flexibility under these conditions (Fig. 3b, c). In these configurations, Ser1438 of ACP_5 points away from PikAIII, which is fully compatible with ACP_5 docking to the KS_6 side entrance of PikAIV for substrate transfer (Dutta *et al.*). This demonstrates the mechanism to maintain the directionality of PKS pathways, because only when the substrate is completely modified is the ACP ejected from the reaction chamber and positioned for transfer to the next module (Fig. 4). Consistent with this mechanism, when NADPH was excluded from a coupled PikAIII/PikAIV assay[14], thus preventing β-hydroxyhexaketide formation, substrate consumption was halved indicating that intermediate transfer from PikAIII to PikAIV is impaired when ACP is sequestered within the reaction chamber (Extended Data Fig. 5).

Our studies capture the travels of PikAIII ACP_5 in the reaction chamber of a complete PKS module and reveal a stunning ACP localization dependent on the identity of the phosphopantetheine-linked polyketide intermediate or extender unit (Fig. 4). The cryo-EM structures identified interaction surfaces for ACP_5 on each of the catalytic domains, different in all cases than predicted sites, and confirmed by site-directed mutagenesis. The interacting surfaces of ACP_5 are generally charge-complementary with partner catalytic domains, and similar to those recently observed in other ACP-enzyme interactions[22–24] (Dutta *et al.*). Interestingly, ACP_5 does not engage in specific protein-protein interactions with catalytic domains unless the appropriate substrate is loaded, indicating that tethered substrate is a primary determinant of ACP_5 localization. However, the high level of ordering observed for ACP does not apply to the post-ACP elements. The post-ACP helices, while essential for PikAIII dimerization, do not appear to be in a fixed position relative to the other PikAIII domains, suggesting that docked or fused downstream modules would also not assume a fixed position relative to the upstream module. Remarkably, the cryo-EM structures also demonstrate the existence of inter-domain cross-talk within the module, evidenced both by the end-to-end flip of the KR_5 that positions its active site to interact with the β-ketohexaketide-loaded ACP and by movements of AT_5 that appear to limit access to the KS_5

active site side entrance. Both structural transitions occur when the module contains pentaketide or hexaketide intermediates, indicating that the operation of the assembly line sets the conformational state of the PKS module and positions the domains for the next catalytic step. This clever design of the PKS module leads to optimal throughput where substrate availability and the rates of catalysis, rather than transfer rates, likely are the limiting steps in the catalytic cycle of type I modular megasynthases. The striking influence of substrate in the positioning and orientation of ACP, KR, and AT has profound implications for the design of PKS modules. Although considerable optimization may be needed in adapting modules to unnatural substrates or in developing effective combinatorial biosynthesis approaches, the detailed insights revealed in this study provide a new structural framework from which to pursue these efforts.

Methods

Design of expression constructs

Construction of expression plasmids for PikAIII (pPikAIII) and PikAIV (pPikAIV)[25] and for PikAIII fused to PikAIV TE (pPikAIII-TE)[26] was described previously. Mutations of PikAIII-TE were made with site directed mutagenesis using the QuikChange Lightning multi-site kit (Strategene). All DNA constructs were confirmed with sequencing. Primers used for site directed mutagenesis are listed below (underlined text indicates mutated base pairs in the site-directed mutagenesis primers):

PikAIIIR747A

TGCGAGGCCGACGGCGTCGCTGCGCGGATCATCCCGGTC

PikAIIIE735A

GGCGACCCGACCCAGATCGCGGAACTCGCCCGCACCTGC

PikAIIIE766R

CGGCAGGTCGAGATCATCAGGAAGGAGCTGGCCGAGGTC

PikAIIIE768R

GTCGAGATCATCGAGAAGAGGCTGGCCGAGGTCCTCGCC

PikAIIIR1133E

CTCGGCAGCCACGCCGCAGAGTGGATGGCCCACCACGGA

PikAIIIH1137E

GCCGCACGCTGGATGGCCGAGCACGGAGCCGAACACCTC

PikAIIIR1308E

GACGACGCGTACTGGCAGGAGCGCGGCATCCGTCCGATG

Expression and Purification

All expression plasmids were expressed in *E. coli* Bap1[27] cells to produce holo ACP. Transformed bacteria were cultured at 37°C to an OD_{600}=1 in 0.5 μL of TB media with 50 μg/ml kanamycin. After incubation at 20°C for 1 hr, cells were induced with 200 μM IPTG and allowed to express for approximately 18 hr.

Cell pellets were re-suspended in 50 mM HEPES pH 7.4 (buffer A), 300 mM NaCl, 10% glycerol containing 0.1 mg/mL lysozyme, 0.05 mg/mL DNase, 2 mM $MgCl_2$ and 20 mM imidazole. Cells were lysed by sonication, centrifuged, and the supernatant was loaded onto a 5-mL His trap column (GE Healthcare). A gradient of 15–300 mM imidazole in buffer A over 10 column volumes was used to elute the proteins.

For the PikAIII, PikAIV, PikAIII-TE proteins used in activity assays, the peak fractions from the His-Trap column were dialyzed overnight into buffer A to remove imidazole and frozen. For PikAIII proteins analyzed with EM, peak fractions from the His column were collected and further purified with a HiPrep 16/60 Sephacryl S300 HR column in buffer A. The peak fractions from the first gel filtration column were collected and further purified on a second HiPrep 16/60 Sephacryl S300 HR column.

Substrate loading of PikAIII constructs

All proteins were dialyzed into 50 mM HEPES pH 7.4, 100 mM NaCl prior to incubation with substrates. For the pentaketide-PikAIII state, 1 μM holo-PikAIII was incubated with 1 mM thiophenol-pentaketide[10] 30 min at room temperature. For the β-ketohexaketide-PikAIII state, 1 μM holo-PikAIII was incubated with 500 μM methylmalonyl-CoA and 1 mM thiophenol-pentaketide 30 min at room temperature. For the β-hydroxyhexaketide-PikAIII state, 1 μM holo-PikAIII was incubated with 1 mM NADPH 10 min at room temperature. Then 500 μM methylmalonyl-CoA and 1 mM thiophenol-pentaketide were added, incubated 30 min at room temperature and frozen.

Mass spectrometric analysis of active site occupancy

Bottom-up liquid chromatography/Fourier transform ion cyclotron resonance mass spectrometry (LC/FT-ICR MS) was used to confirm the presence or absence of substrate in each domain of pentaketide-PikAIII, β-ketohexaketide-PikAIII, and β-hydroxyhexaketide-PikAIII. Loading reactions were as described above except 2 μM holo-PikAIII was used and substrate concentrations were increased accordingly. 25 μL of each loading reaction were diluted with 20 μL 250 mM ammonium bicarbonate (pH 8.0). Trypsin in 50 mM acetic acid was added in an enzyme:substrate ratio of 1:10. Proteolysis was allowed to proceed for 15 min at 37 °C followed by addition of formic acid (pH 4). Samples were stored at −20 °C until analysis.

45 μL sample were injected onto a Synergi Hydro C18 hydrophilically endcapped 1 × 150 mm column with 4 μm particles (Phenomenex, Torrance, CA). A gradient was generated on an Agilent (Santa Clara, CA) 1100 HPLC. The gradient was as follows (with isocratic elution between 40 and 50 min): 0 (98,2), 20 (70,30), 40 (50,50), 50 (50,50), 55 (30,70), 70 (2,98). Values are provided as time (%A, %B) over a total run time of 90 min. Flow was at

50 μL/min and was diverted for the first 5 min of the run. Buffer A was 0.1% formic acid (ThermoFisher Scientific, Waltham, MA) in HPLC-grade water (ThermoFisher Scientific), and buffer B was 0.1% formic acid in acetonitrile (ThermoFisher Scientific). The LC was coupled to a quadrupole FTICR-MS (SolariX with 7T magnet, Bruker Daltonics, Billerica, MA). Data were gathered from m/z 200–2000 in positive ion mode. Electrospray was conducted at 4500 V with four scans per spectrum and a 256k transient. External ion accumulation in a hexapole was 0.2 s and there was 1 ICR fill prior to excitation and detection. External calibration utilized HP-mix (Agilent). PikAIII peptide products were detected over three samples in separate runs.

Sample preparation and cryo-EM imaging

Sample quality and homogeneity was evaluated by conventional negative staining[28]. For cryo-EM, sample preparation and image acquisition was performed as described in the accompanying paper (Dutta, *et al.*). Substrate incubation conditions for each sample characterized by cryo-EM are described above.

Image processing and 3D reconstructions

Image processing and 3D reconstructions were performed as described in the accompanying paper (Dutta, *et al.*) using EMAN (1.9)[29]. A 30-Å low-pass filtered map of MM-PikAIII (Dutta et al.) was used as the initial model for iterative projection matching and 3D reconstructions of pentaketide-PikAIII. The final map of pentaketide-PikAIII was filtered to 30-Å and used as the initial reference for 3D reconstructions of β-ketohexaketide-PikAIII and for all three conformations of β-hydroxyhexaketide-PikAIII. All refinements were performed based on the same procedure described in the accompanying paper (Dutta, *et al.*) and with final angular steps of 2°–5°. The numbers of particle projections used for the final 3D reconstructions are listed in Extended Data Fig. 2d.

In initial reconstructions of β-hydroxyhexaketide-PikAIII we observed three separate densities corresponding to the ACP, all attached at the bottom of KR and outside of the reaction chamber. To separate the particle projections corresponding to each ACP state we employed multiple reference-supervised classification[20, 21]. To this end we produced three initial models that differed only in the ACP position by docking the structures of DEBS module 5 KS and AT[11], DEBS module 1 KR[12] and DEBS module 2 ACP[13] in the corresponding densities of the initial reconstruction. We proceeded with multiple reference-supervised classification by subjecting the full dataset of 56,429 projections to the *multirefine* routine in EMAN (1.9)[29] using the three above models as references. In this way the particle projections were classified into three categories according to their cross-correlation with reprojections of the three references of β-hydroxyhexaketide-PikAIII. The number of particles in each category is provided in Extended Data Fig. 2d. In the next step, we used the separated particle datasets to calculate the three independent 3D reconstructions using the 30-Å low pass filtered EM map of pentaketide-PikAIII as an initial reference, as described above.

The validation of the reconstruction scheme and EM maps has been extensively described in the accompanying manuscript by Dutta *et al*. Besides the conventional full dataset

refinements we additionally ran independent gold-standard[30] refinements of half data for pentaketide-PikAIII and β-ketohexaketide-PikAIII employing 50-Å filtered EM maps as initial reference. Resolution calculations were based on conventional "even/odd" Fourier Shell Correlation (FSC) and also gold standard FSC measurements in EMAN. The FSC plots for all 3D reconstructions are provided in Extended Data Fig. 2. Briefly, the gold standard procedure shows a resolution of 7.9 Å for pentaketide-PikAIII and 8.2 Å for β-ketohexaketide-PikAIII at FSC=0.143[30], in good agreement with the conventional 0.5 FSC values of 7.9 Å and 7.8 Å, respectively (Extended Data Fig. 2a, b, d). Consistent with these measurements, the agreement between the map from the conventional procedure and the map resulting from averaging the two gold standard half-maps[31] of pentaketide-PikAIII and β-ketohexaketide-PikAIII extends to 8.0 Å and 8.2 Å at 0.5 FSC, respectively (Extended Data Fig. 2d). Gold standard resolution calculations were not performed for the three β-hydroxyhexaketide-PikAIII conformer maps due to the limited number projections included in half-datasets (Extended Data Fig. 2d). The resolution of the β-hydroxyhexaketide-PikAIII conformer i, ii and iii maps was assessed by conventional FSC measurements and was found to be 10.7 Å, 11.0 Å, and 11.6 Å with the 0.5 FSC criterion, respectively (Extended Data Fig. 2c, d). Finally, we applied high-resolution phase randomization tests[32] for pentaketide-PikAIII and β-ketohexaketide-PikAIII reconstructions and did not detect any obvious over-fitting (noise refinement) (Extended Data Fig. 2a, b). Thus, independent FSC calculations and phase randomization tests exclude any detectable map over-refinement (see also Dutta *et al.*). The final 3D EM maps were sharpened using EMBFACTOR[33, 34] and subsequently filtered according to their indicated resolution range.

Modeling and map visualization

The crystal structures of DEBS module 5 KS dimer (PDBID: 2HG4)[11], AT monomer (PDBID: 2HG4)[11] and DEBS module 1 KR monomer (PDBID: 2FR0)[12] and the NMR structure of DEBS module 2 ACP (PDBID: 2JU1)[13] were independently fit in the EM maps as rigid bodies using the *fit in map* routine in CHIMERA[35] (for details see the accompanying paper by Dutta *et al.*). As the PikAIII KR_5 domain is an A-type KR, we fit crystal structures of both an A-type[36] and a B-type KR[12] to the EM density. The highly similar KRs both fit well, but the B-type KR was a better fit in regions with low sequence identity and was used for all models.

Enzyme Assays

PikAIII-TE and PikAIII/PikAIV assays were described previously[14, 15]. Either 1 μM PikAIII-TE or 1 μM PikAIII and 1 μM PikAIV was added to a 100-μL reaction mixture containing 0.5 mM $NADP^+$, 0.5 U/mL glucose-6-phosphate dehydrogenase, 5 mM glucose-6-phosphate in 400 mM sodium phosphate pH 7.2, 20% glycerol, 5 mM NaCl. This mixture was incubated for 10 min at room temperature and the reaction was initiated by addition of 1 mM thiophenol-pentaketide[10], 8 mM 2-vinylpyridine, and 20 mM methylmalonyl-SNAC. Following a 1-hr incubation at room temperature, the reaction was quenched by addition of a three-fold excess of methanol, vortexed, incubated for 15 min at −20°C, and centrifuged. The supernatant was analyzed by reverse-phase HPLC on a Luna C18(2) (5μm, 250 × 4.6mm) column (Phenomenex) with a flow rate of 1.5mL/min and by following this protocol: 5% solvent B (acetonitrile with 0.1% formic acid) for 1 min, 5–

100% solvent B for 10 min, 100% solvent B for 4 min, and 5% solvent B for 2.5 min. Solvent A was water with 0.1% formic acid. Authentic standards confirmed the elution time of 10-dml and nbl. For the PikAIII-TE mutants, peak areas of 10-dml normalized to the values for wild-type PikAIII-TE were used to assess activity. For the PikAIII/PikAIV assays lacking NADPH, the peak areas of starting material were normalized to values for a reaction that lacked enzyme and compared to a reaction that contained NADPH.

Acknowledgments

This work was supported by the Pew Scholar Program in Biomedical Sciences (G.S.), the University of Michigan Biological Sciences Scholars Program (G.S.), Rackham Merit and American Foundation for Pharmaceutical Education pre-doctoral fellowships (D.A.H.), an NRSA postdoctoral fellowship (J.A.C.), the Life Sciences Research Foundation (A.R.H.N), NIH grant 1R21CA138331-01A1 (K.H.), GM076477 (D.H.S. and J.L.S.), and DK042303 (J.L.S.) and the Hans W. Vahlteich Professorship (to D.H.S.).

References

1. Newman DJ, Cragg GM. Natural products as sources of new drugs over the 30 years from 1981 to 2010. J Nat Prod. 2012; 75:311–335. [PubMed: 22316239]
2. Kittendorf JD, Sherman DH. Developing tools for engineering hybrid polyketide synthetic pathways. Curr Opin Biotechnol. 2006; 17:597–605. [PubMed: 17046237]
3. Walsh CT. Combinatorial biosynthesis of antibiotics: challenges and opportunities. Chembiochem. 2002; 3:125–134. [PubMed: 11921390]
4. Menzella HG, Reeves CD. Combinatorial biosynthesis for drug development. Curr Opin Microbiol. 2007; 10:238–245. [PubMed: 17553731]
5. Menzella HG, Carney JR, Santi DV. Rational design and assembly of synthetic trimodular polyketide synthases. Chem Biol. 2007; 14:143–151. [PubMed: 17317568]
6. Menzella HG, Reid R, Carney JR, Chandran SS, Reisinger SJ, Patel KG, Hopwood DA, Santi DV. Combinatorial polyketide biosynthesis by de novo design and rearrangement of modular polyketide synthase genes. Nat Biotechnol. 2005; 23:1171–1176. [PubMed: 16116420]
7. Sherman DH. The Lego-ization of polyketide biosynthesis. Nat Biotechnol. 2005; 23:1083–1084. [PubMed: 16151397]
8. Fischbach MA, Walsh CT. Assembly-line enzymology for polyketide and nonribosomal Peptide antibiotics: logic, machinery, and mechanisms. Chem Rev. 2006; 106:3468–3496. [PubMed: 16895337]
9. Xue Y, Zhao L, Liu HW, Sherman DH. A gene cluster for macrolide antibiotic biosynthesis in Streptomyces venezuelae: architecture of metabolic diversity. Proc Natl Acad Sci U S A. 1998; 95:12111–12116. [PubMed: 9770448]
10. Hansen DA, Rath CM, Eisman EB, Narayan AR, Kittendorf JD, Mortison JD, Yoon YJ, Sherman DH. Biocatalytic synthesis of pikromycin, methymycin, neomethymycin, novamethymycin, and ketomethymycin. J Am Chem Soc. 2013; 135:11232–11238. [PubMed: 23866020]
11. Tang Y, Kim CY, Mathews II, Cane DE, Khosla C. The 2.7-Å crystal structure of a 194-kDa homodimeric fragment of the 6-deoxyerythronolide B synthase. Proc Natl Acad Sci U S A. 2006; 103:11124–11129. [PubMed: 16844787]
12. Keatinge-Clay AT, Stroud RM. The structure of a ketoreductase determines the organization of the beta-carbon processing enzymes of modular polyketide synthases. Structure. 2006; 14:737–748. [PubMed: 16564177]
13. Alekseyev VY, Liu CW, Cane DE, Puglisi JD, Khosla C. Solution structure and proposed domain domain recognition interface of an acyl carrier protein domain from a modular polyketide synthase. Protein Sci. 2007; 16:2093–2107. [PubMed: 17893358]
14. Aldrich CC, Beck BJ, Fecik RA, Sherman DH. Biochemical investigation of pikromycin biosynthesis employing native penta- and hexaketide chain elongation intermediates. J Am Chem Soc. 2005; 127:8441–8452. [PubMed: 15941278]

15. Aldrich CC, Venkatraman L, Sherman DH, Fecik RA. Chemoenzymatic synthesis of the polyketide macrolactone 10-deoxymethynolide. J Am Chem Soc. 2005; 127:8910–8911. [PubMed: 15969542]
16. Wong FT, Chen AY, Cane DE, Khosla C. Protein-protein recognition between acyltransferases and acyl carrier proteins in multimodular polyketide synthases. Biochemistry. 2010; 49:95–102. [PubMed: 19921859]
17. Caffrey P. Conserved amino acid residues correlating with ketoreductase stereospecificity in modular polyketide synthases. Chembiochem. 2003; 4:654–657. [PubMed: 12851937]
18. Keatinge-Clay AT. A tylosin ketoreductase reveals how chirality is determined in polyketides. Chem Biol. 2007; 14:898–908. [PubMed: 17719489]
19. Bonnett SA, Whicher JR, Papireddy K, Florova G, Smith JL, Reynolds KA. Structural and stereochemical analysis of a modular polyketide synthase ketoreductase domain required for the generation of a cis-alkene. Chem Biol. 2013; 20:772–783. [PubMed: 23790488]
20. Lyon AM, Dutta S, Boguth CA, Skiniotis G, Tesmer JJ. Full-length Gα(q)-phospholipase C-β3 structure reveals interfaces of the C-terminal coiled-coil domain. Nat Struct Mol Biol. 2013; 20:355–362. [PubMed: 23377541]
21. Strunk BS, Loucks CR, Su M, Vashisth H, Cheng S, Schilling J, Brooks CL 3rd, Karbstein K, Skiniotis G. Ribosome assembly factors prevent premature translation initiation by 40S assembly intermediates. Science. 2011; 333:1449–1453. [PubMed: 21835981]
22. Nguyen C, Haushalter RW, Lee DJ, Markwick PR, Bruegger J, Caldara-Festin G, Finzel K, Jackson DR, Ishikawa F, O'Dowd B, McCammon JA, Opella SJ, Tsai SC, Burkart MD. Trapping the dynamic acyl carrier protein in fatty acid biosynthesis. Nature. 2014; 505:427–431. [PubMed: 24362570]
23. Masoudi A, Raetz CR, Zhou P, Pemble CWt. Chasing acyl carrier protein through a catalytic cycle of lipid A production. Nature. 2014; 505:422–426. [PubMed: 24196711]
24. Bunkoczi G, Pasta S, Joshi A, Wu X, Kavanagh KL, Smith S, Oppermann U. Mechanism and substrate recognition of human holo ACP synthase. Chem Biol. 2007; 14:1243–1253. [PubMed: 18022563]
25. Beck BJ, Aldrich CC, Fecik RA, Reynolds KA, Sherman DH. Iterative chain elongation by a pikromycin monomodular polyketide synthase. J Am Chem Soc. 2003; 125:4682–4683. [PubMed: 12696866]
26. Yin Y, Lu H, Khosla C, Cane DE. Expression and kinetic analysis of the substrate specificity of modules 5 and 6 of the picromycin/methymycin polyketide synthase. J Am Chem Soc. 2003; 125:5671–5676. [PubMed: 12733905]
27. Pfeifer BA, Admiraal SJ, Gramajo H, Cane DE, Khosla C. Biosynthesis of complex polyketides in a metabolically engineered strain of E. coli. Science. 2001; 291:1790–1792. [PubMed: 11230695]
28. Ohi M, Li Y, Cheng Y, Walz T. Negative staining and image classification -powerful tools in modern electron microscopy. Biol Proced Online. 2004; 6:23–34. [PubMed: 15103397]
29. Ludtke SJ, Baldwin PR, Chiu W. EMAN: semiautomated software for high-resolution single-particle reconstructions. J Struct Biol. 1999; 128:82–97. [PubMed: 10600563]
30. Scheres SH, Chen S. Prevention of overfitting in cryo-EM structure determination. Nat Methods. 2012; 9:853–854. [PubMed: 22842542]
31. Li X, Mooney P, Zheng S, Booth CR, Braunfeld MB, Gubbens S, Agard DA, Cheng Y. Electron counting and beam-induced motion correction enable near-atomic-resolution single-particle cryo-EM. Nat Methods. 2013; 10:584–590. [PubMed: 23644547]
32. Chen S, McMullan G, Faruqi AR, Murshudov GN, Short JM, Scheres SH, Henderson R. High-resolution noise substitution to measure overfitting and validate resolution in 3D structure determination by single particle electron cryomicroscopy. Ultramicroscopy. 2013; 135:24–35. [PubMed: 23872039]
33. Fernandez JJ, Luque D, Caston JR, Carrascosa JL. Sharpening high resolution information in single particle electron cryomicroscopy. J Struct Biol. 2008; 164:170–175. [PubMed: 18614378]
34. Rosenthal PB, Henderson R. Optimal determination of particle orientation, absolute hand, and contrast loss in single-particle electron cryomicroscopy. J Mol Biol. 2003; 333:721–745. [PubMed: 14568533]

35. Pettersen EF, Goddard TD, Huang CC, Couch GS, Greenblatt DM, Meng EC, Ferrin TE. UCSF Chimera--a visualization system for exploratory research and analysis. J Comput Chem. 2004; 25:1605–1612. [PubMed: 15264254]

36. Zheng J, Taylor CA, Piasecki SK, Keatinge-Clay AT. Structural and functional analysis of A-type ketoreductases from the amphotericin modular polyketide synthase. Structure. 2010; 18:913–922. [PubMed: 20696392]

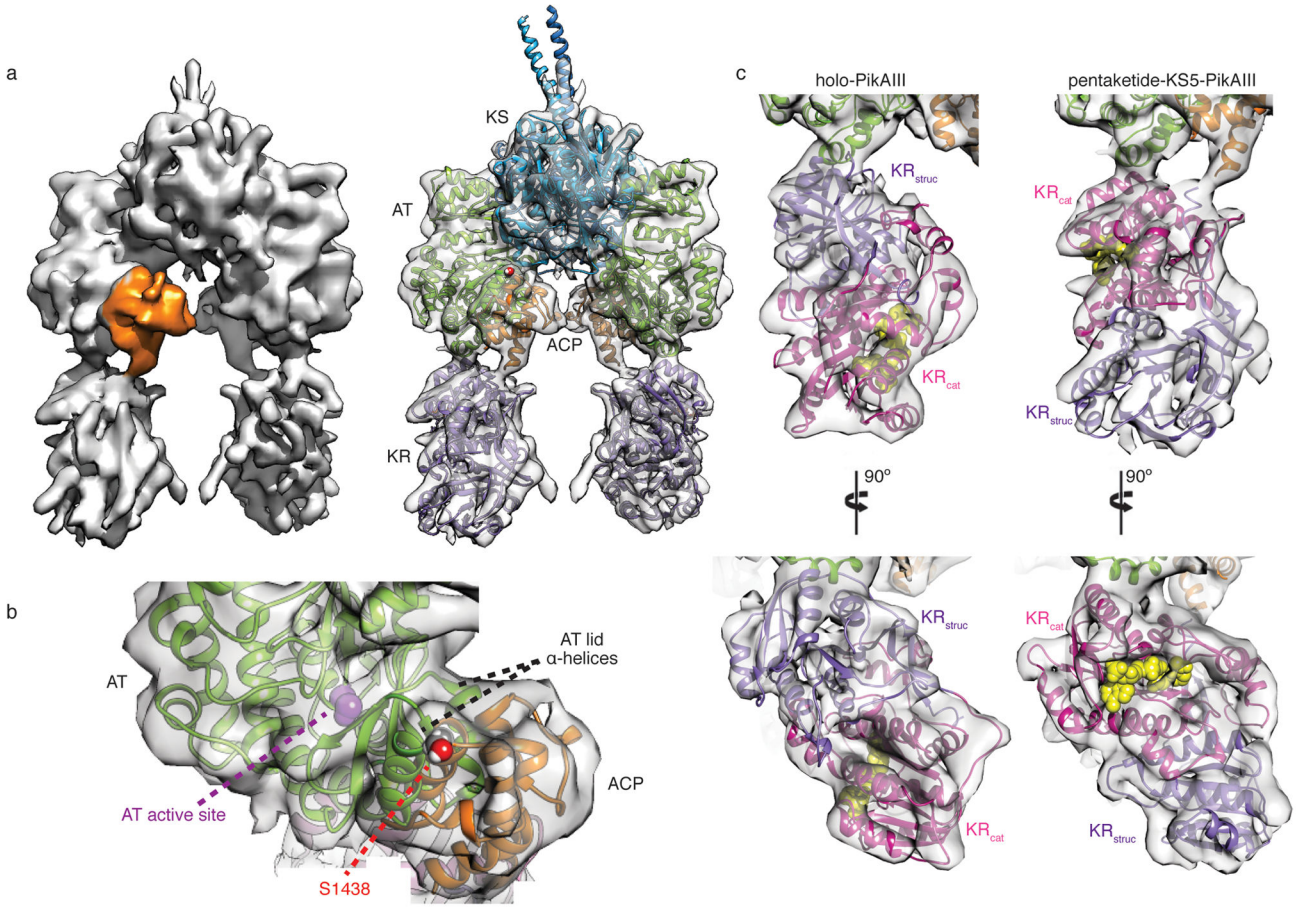

Figure 1.

Cryo-EM structure of pentaketide-KS_5-PikAIII. **a**, Solid rendering (left) and transparent representation with modeled structures (right) of the pentaketide-KS_5-PikAIII cryo-EM map. **b**, Interface of AT[11] and ACP[13] docked within the cryo-EM density. ACP helix 2 (residues 1439–1452) contacts the two AT lid helices (residues 701–709 and 732–744). The phosphopantetheinylated Ser1438 of ACP is 35 Å from the AT active site. **c**, Comparison of the KR structure[12] docked in the cryo-EM map for holo-PikAIII and pentaketide-KS_5-PikAIII. The dramatic rearrangement upon pentaketide-KS formation brings two helices (residues 1126–1138, 1156–1166) of the KR catalytic sub-domain (KR_{cat}, magenta) in contact with an AT helix (residues 760–775) and moves the structural sub-domain of KR (KR_{struc}, purple) away from AT.

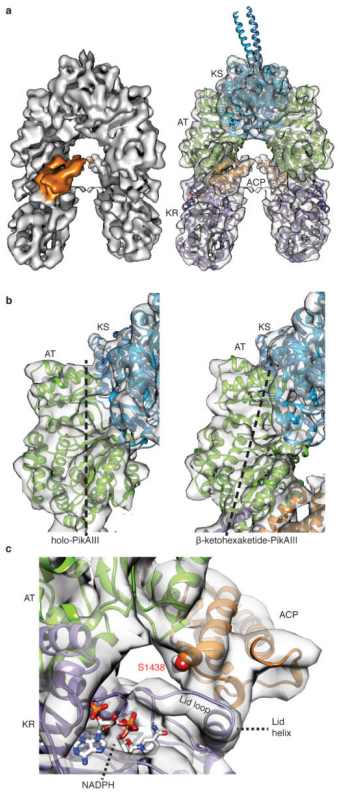

Figure 2.

Cryo-EM structure of β-ketohexaketide-PikAIII. **a**, Solid rendering and transparent representation with modeled structures of the β-ketohexaketide-PikAIII cryo-EM map. **b**, Comparison of the KS-AT interface between holo-PikAIII (left) and β-ketohexaketide-PikAIII (right). Polyketide chain extension results in an 8-Å shift and rotation of AT towards the KS. **c**, ACP interaction with KR. ACP interacts with the KR lid helix (residues 1302–1309) and lid loop (1293–1301) to position ACP Ser1438 near the NADPH binding cleft.

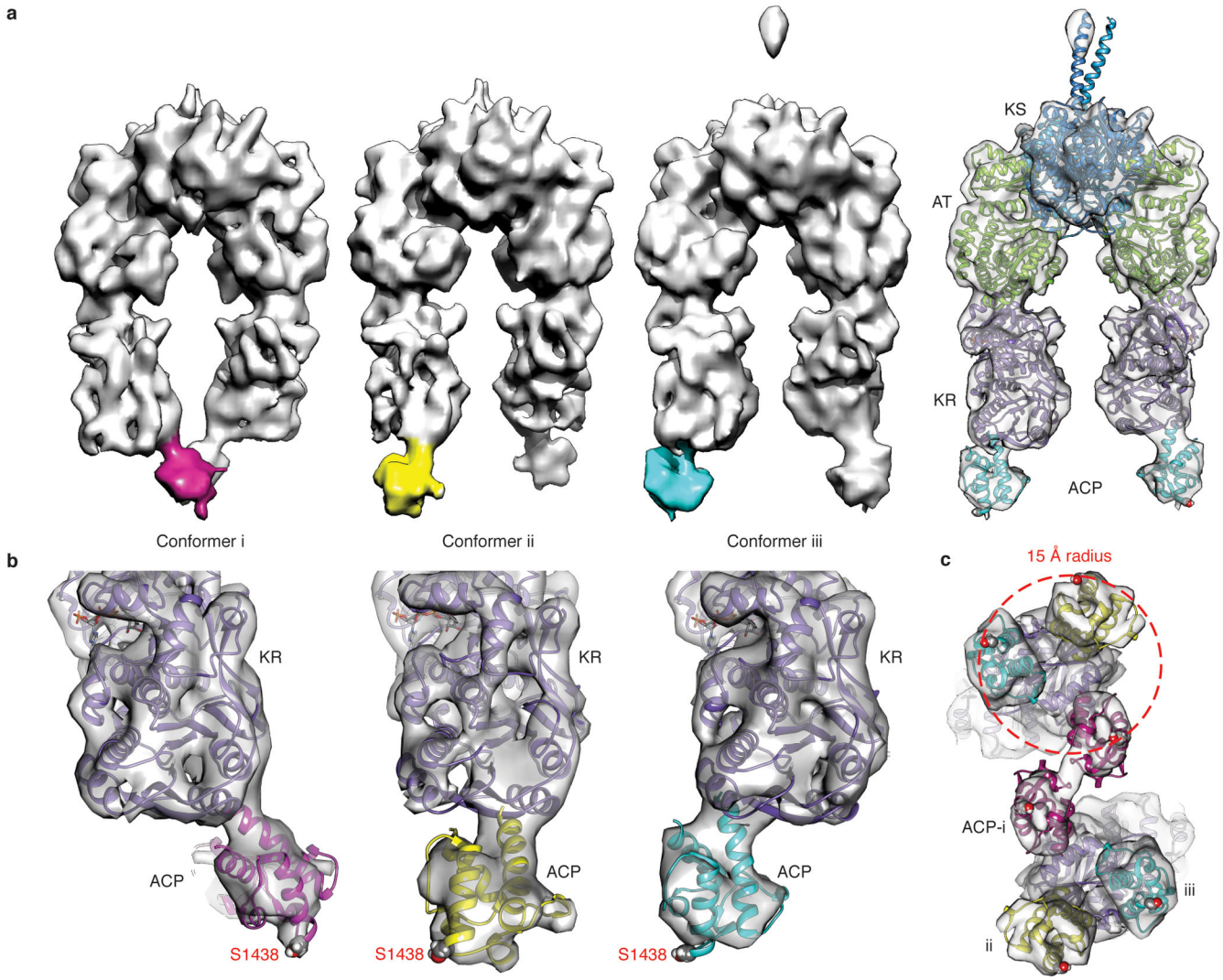

Figure 3.

Cryo-EM structures of β-hydroxyhexaketide-PikAIII. **a**, Solid rendering of cryo-EM maps for the three conformers of β-hydroxyhexaketide-PikAIII. The ACP density is differentially colored with magenta, yellow, and cyan. The panel on the right shows a transparent representation with modeled structures of the adjacent β-hydroxyhexaketide-PikAIII conformer. **b**, Docking of the ACP structure[13] in the corresponding density map of each β-hydroxyhexaketide-PikAIII conformer shows that Ser1438 invariably points away from the module. The ACP structures are colored according to the conformers in panel (a). **c**, Bottom view of overlay of the three cryo-EM maps of β-hydroxyhexaketide-PikAIII. The three different ACP positions cover a surface with a radius of 15 Å.

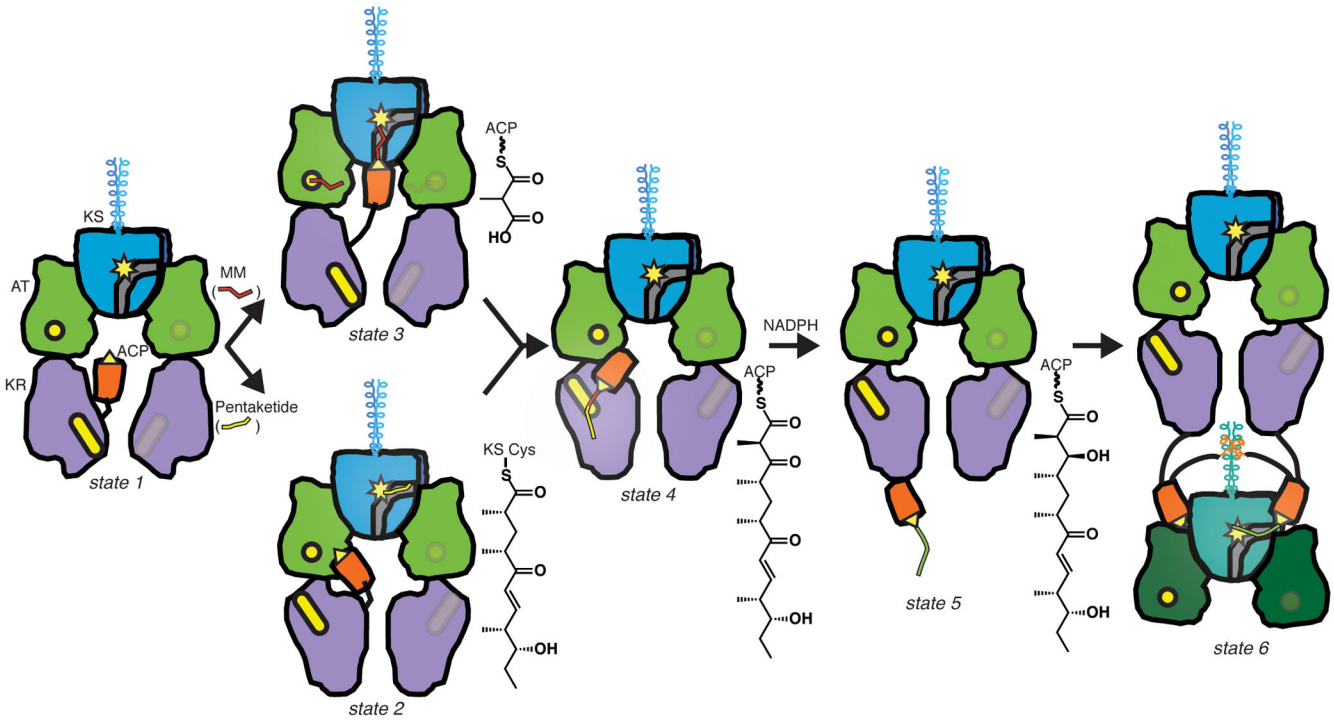

Figure 4.

Schematic of substrate processing in PikAIII. Transfer of the upstream intermediate (pentaketide, yellow line) to the KS domain (blue with yellow active site) of holo-PikAIII (state 1) induces an end-to-end flip of the KR domain (purple, yellow active site) and positions the ACP domain (orange, yellow active serine) at the AT domain (green, yellow active site) (state 2). Methylmalonyl (MM, red line) loading positions the ACP at the bottom entrance of the KS (state 3). KS-catalyzed extension of the pentaketide to a β-ketohexaketide (red-yellow line) positions the ACP at the KR domain (state 4). KR-catalyzed reduction of the β-ketohexaketide to β-hydroxyhexaketide (green line) ejects the ACP out of the central chamber (state 5) and into position for intermediate transfer to PikAIV (state 6).